Geodynamic evolution of the West African Craton at the Archean-Paleoproterozoic transition in the Sassandra-Cavally domain (South-West Côte d'Ivoire)

Augustin Yao Koffi

Félix Houphouet-Boigny University, Abidjan-Cocody, UFR-STRM, 22 BP 582 Abidjan 22, Côte d'Ivoire

Collaborators

Lenka Baratoux, Pavel Pitra, Alain Nicaise Kouamelan, Olivier Vanderhaeghe, Nicolas Thébaud, Olivier Bruguier, Sylvain Block, Hervé Jean-Luc Fossou Kouadio, Anthony I.S. Kemp[b], Noreen J. Evans

INTRODUCTION

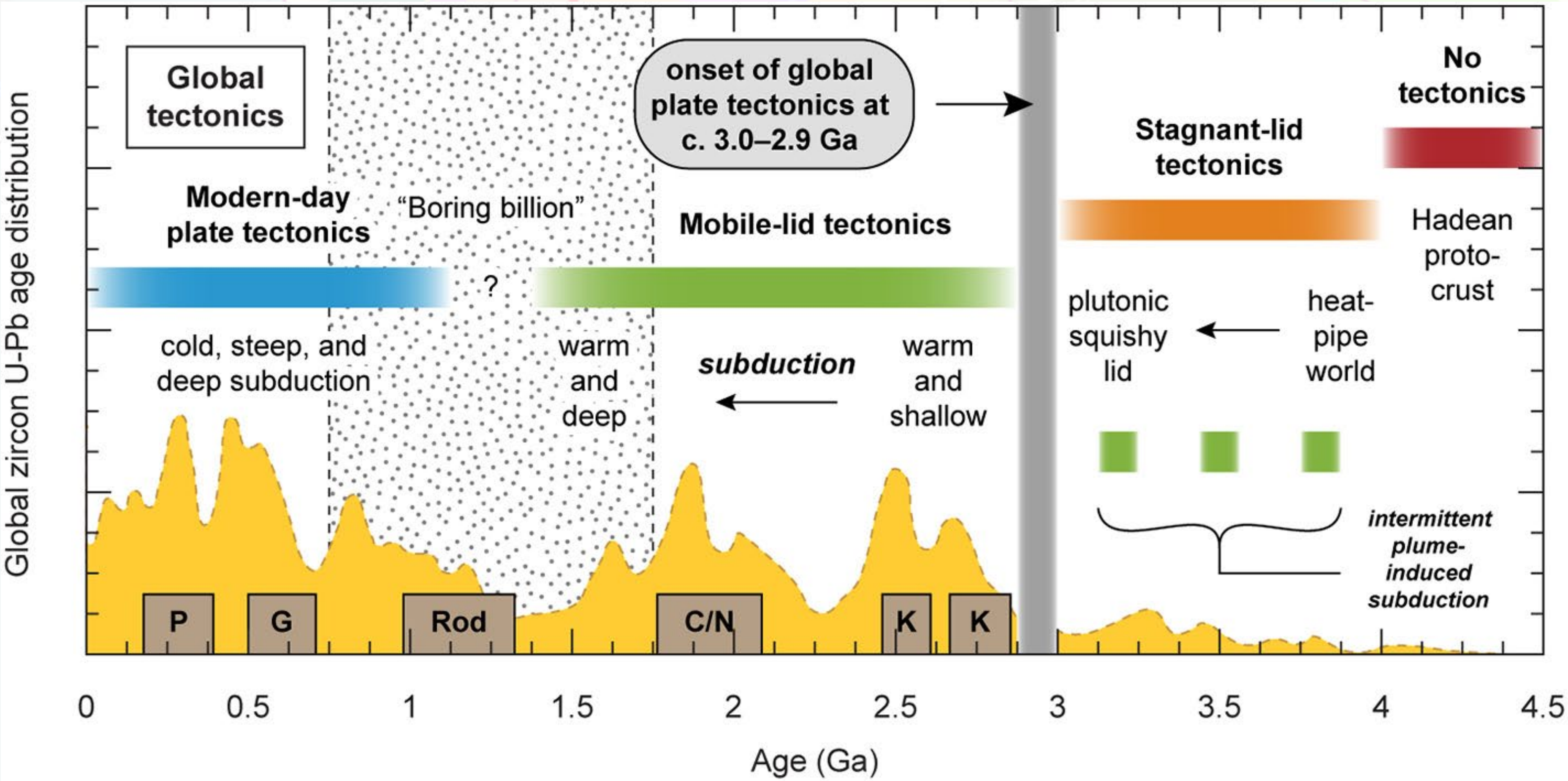

Summary diagram showing the evolution of global tectonics through time as constrained by the various lines of evidence discussed in this review. Global archive of zircon U–Pb ages is from Vermeesch (2012) and brown boxes denote supercontinent events: P = Pangea; G = Gondwana; Rod = Rodinia; C/N = Columbia/Nuna; K = Kenorland. Modified after Palin et al. (2020).

Discuss the thermal and tectonic regime and timing of the Eburnean reworking of the Archean crust.

INTRODUCTION

Paleozoic (0.54 – 0.36 Ga)

Neoproterozoic (1.2 – 0.54 Ga)

Paleoproterozoic (2.3 – 1.9 Ga)

Archean (3.4 – 2.5 Ga)

Study area

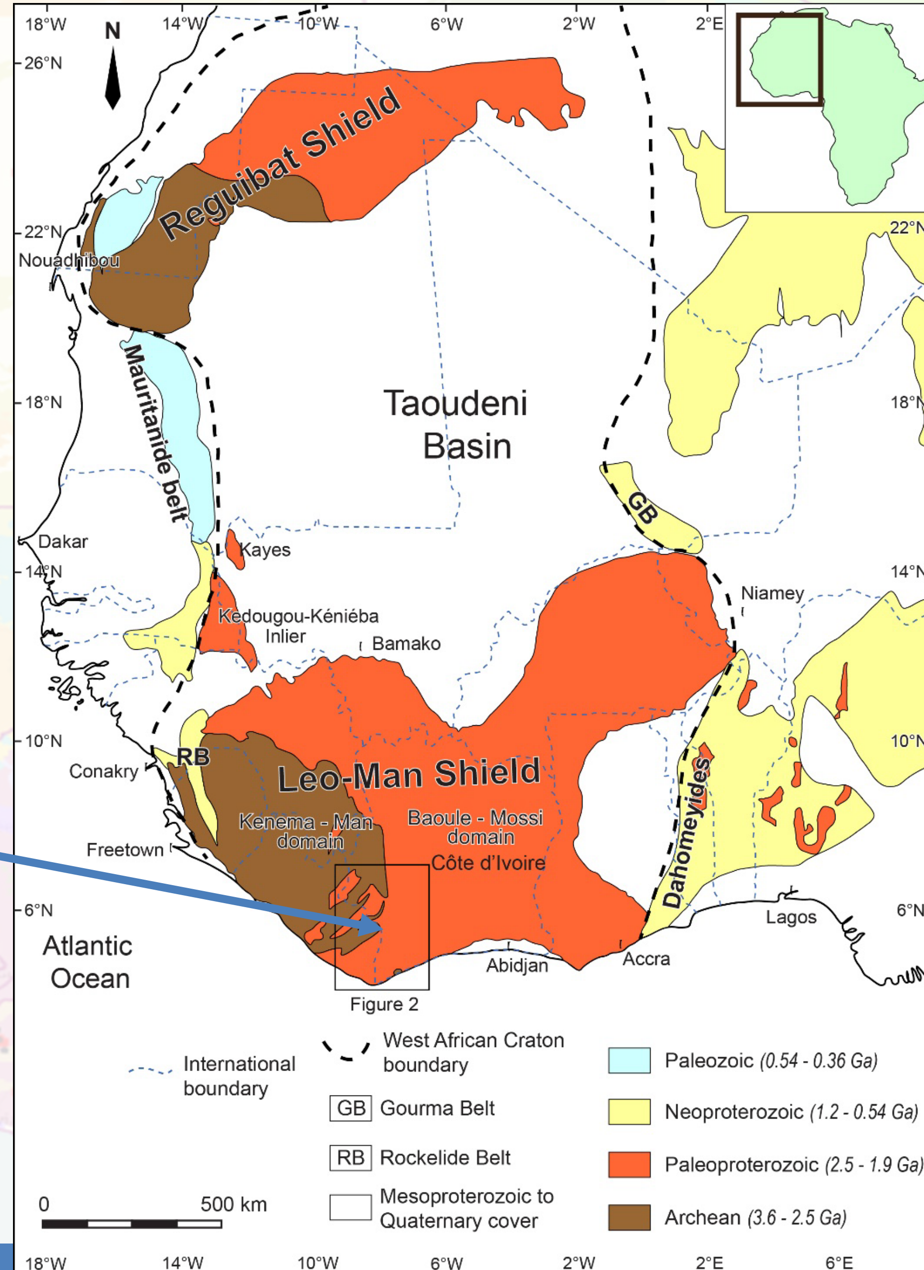

Geological sketch map of the West African Craton (modified after the BRGM SIG Africa map and Ennih and Liégeois, 2008; Berger et al., 2013; Thiéblemont, 2016). The position of the present-day margins of the craton is constrained by geophysics (Jessell et al., 2015).

METHODOLOGY

- ✓ Structural analysis
- ✓ Metamorphic petrology

Theriak - Domino

(de Capitani, 1994)

- ✓ U-Pb and Lu-Hf geochronology on zircon

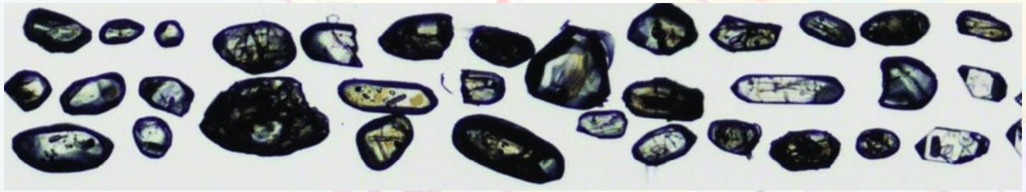

- ✓ U–Pb *in situ* dating of monazite

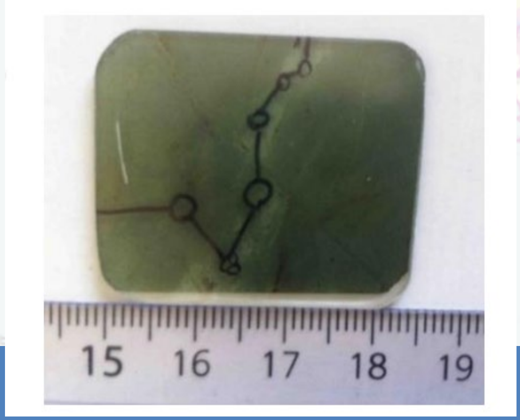

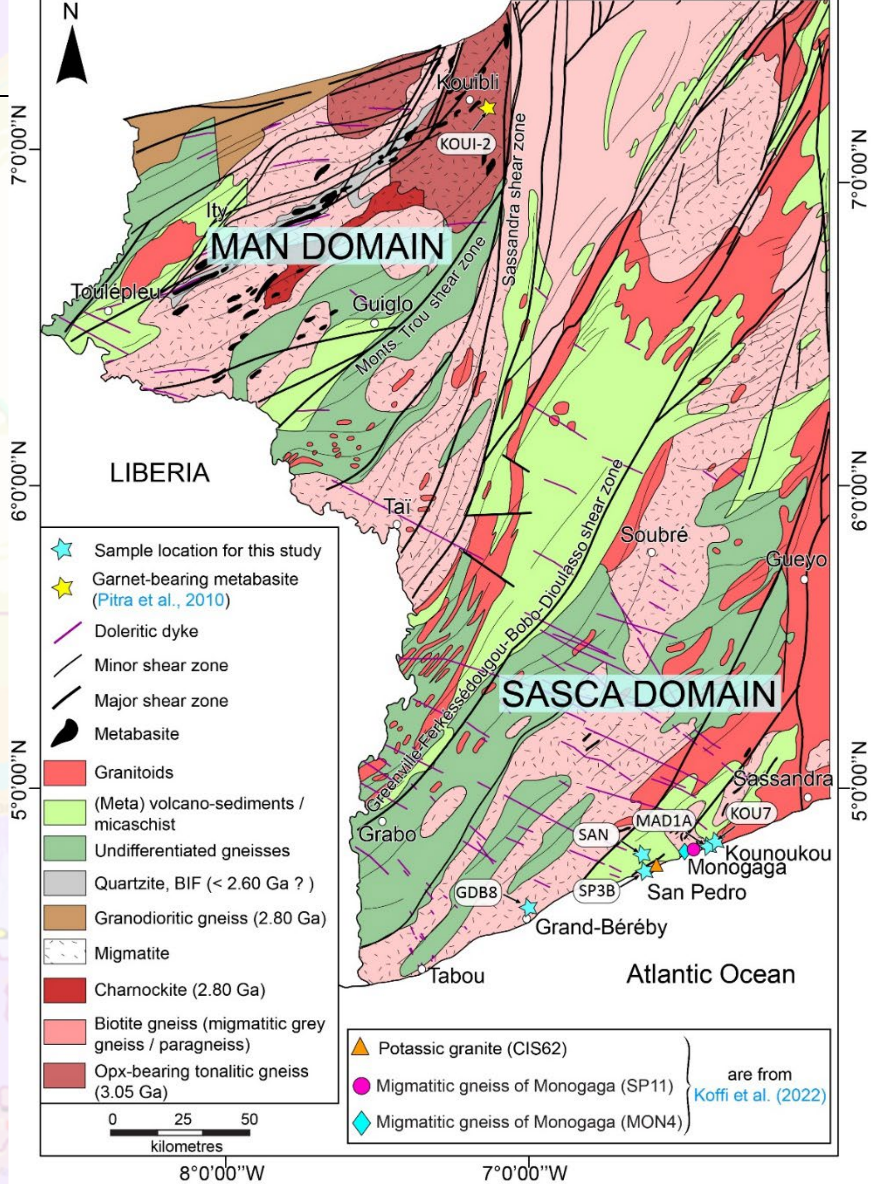

Litho-structural map of the SW of Côte d'Ivoire (modified after Tagini, 1971; Papon, 1973; Pitra et al., 2010; WAXI report, AMIRA Global, 2018).

RESULTS

❖ Petro-structural and mineral chemistry

✓ Garnet–cordierite–sillimanite migmatitic paragneiss (GDB8)

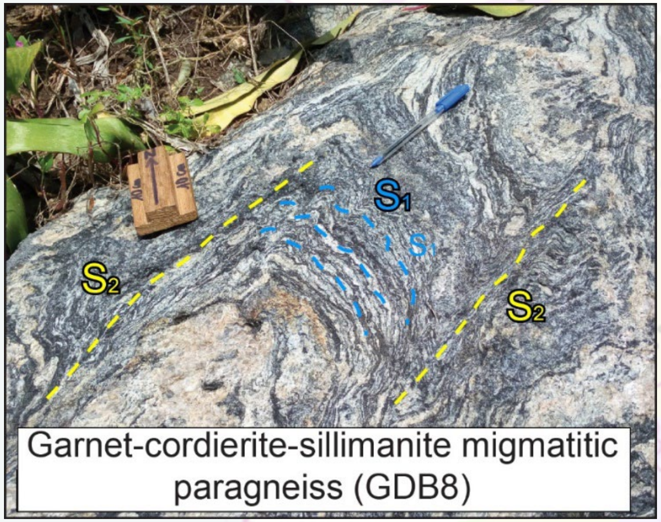

Garnet-cordierite-sillimanite migmatitic paragneiss (GDB8)

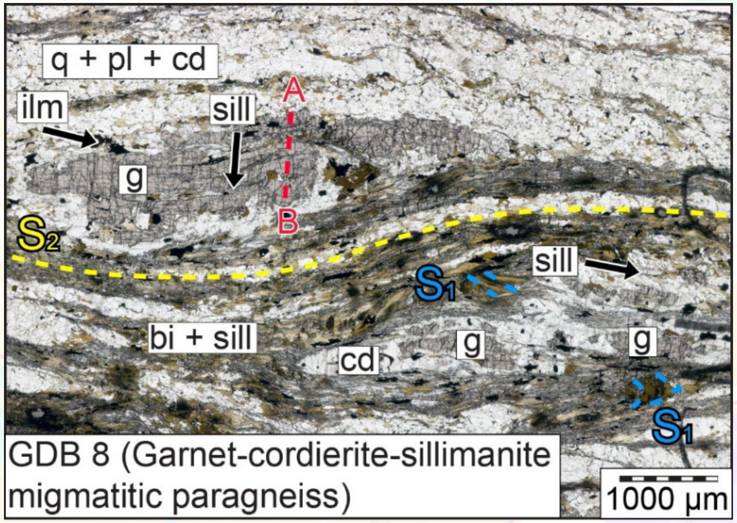

GDB 8 (Garnet-cordierite-sillimanite migmatitic paragneiss)

✓ Migmatitic grey gneiss (SP3B)

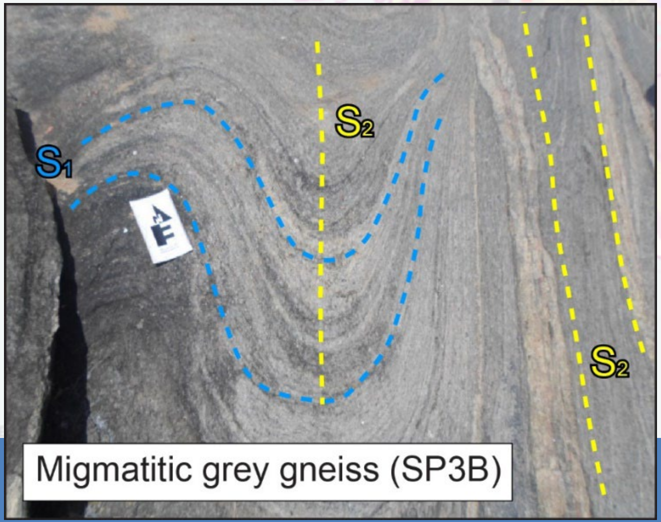

Migmatitic grey gneiss (SP3B)

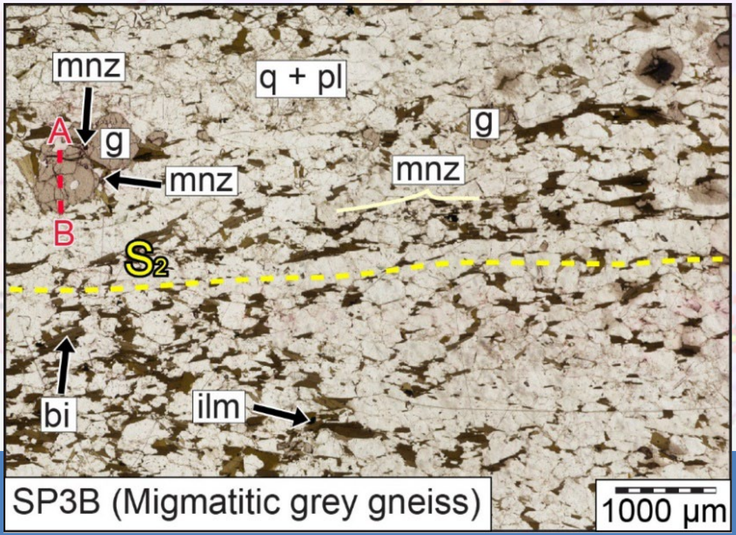

SP3B (Migmatitic grey gneiss)

RESULTS

❖ Petro-structural and mineral chemistry

✓ Staurolite-bearing micaschist (SAN)

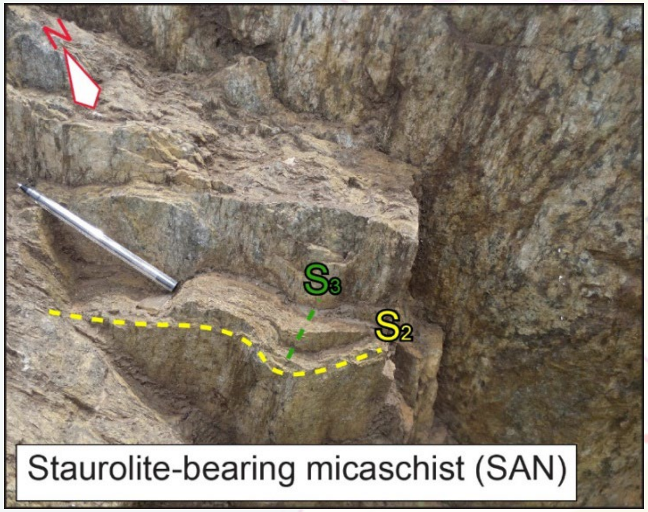

Staurolite-bearing micaschist (SAN)

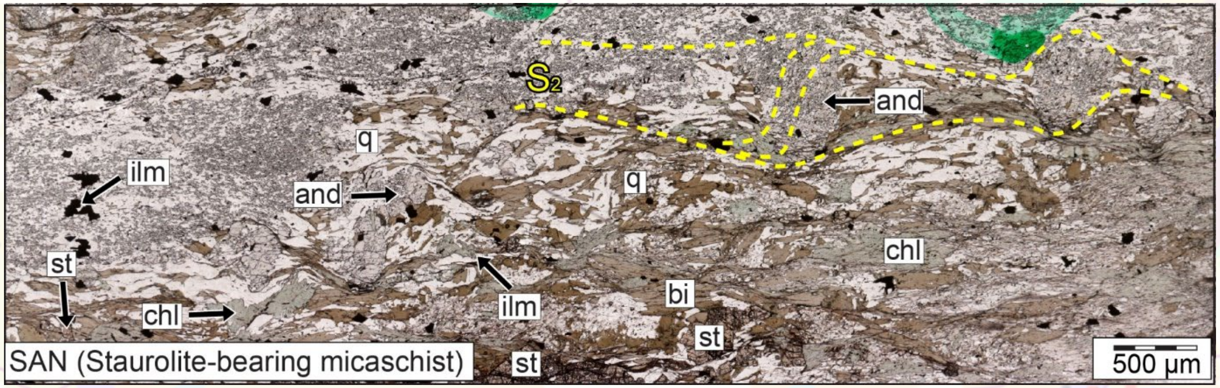

SAN (Staurolite-bearing micaschist)

✓ Garnet–sillimanite–cordierite micaschist (MAD1A)

Garnet-sillimanite-cordierite micaschist (MAD1A)

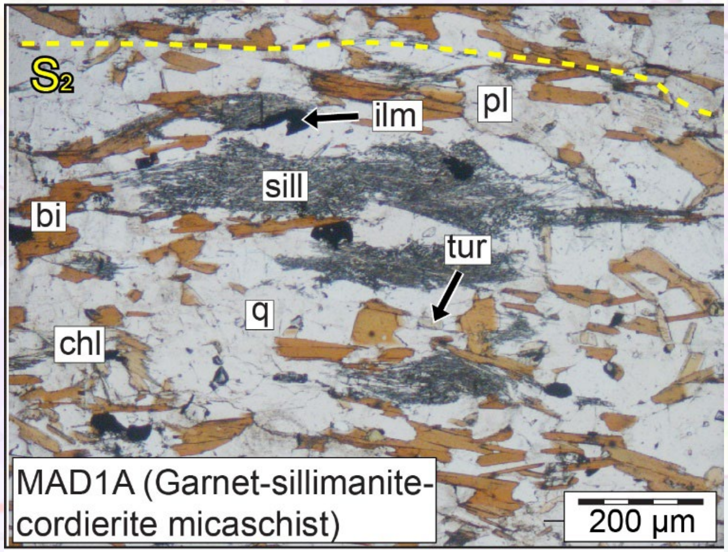

MAD1A (Garnet-sillimanite-cordierite micaschist)

RESULTS

❖ Petro-structural and mineral chemistry

✓ Garnet–staurolite-bearing micaschist (KOU7)

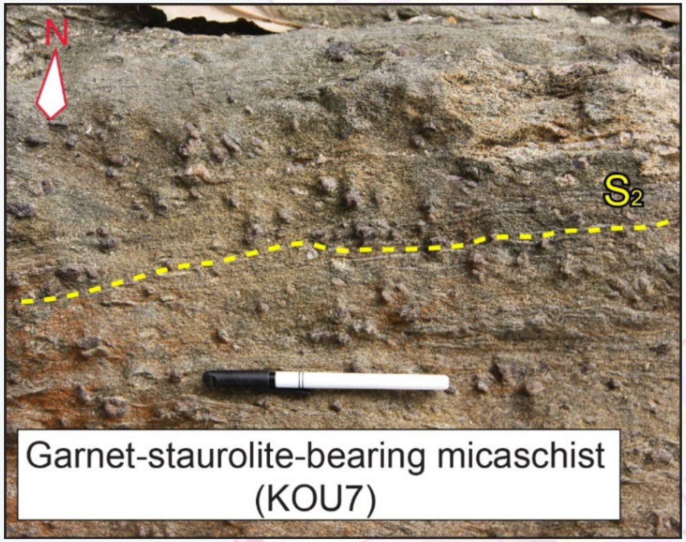

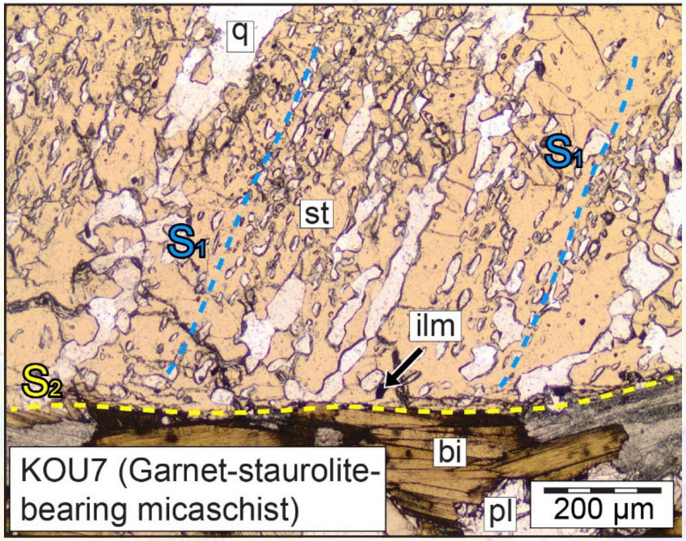

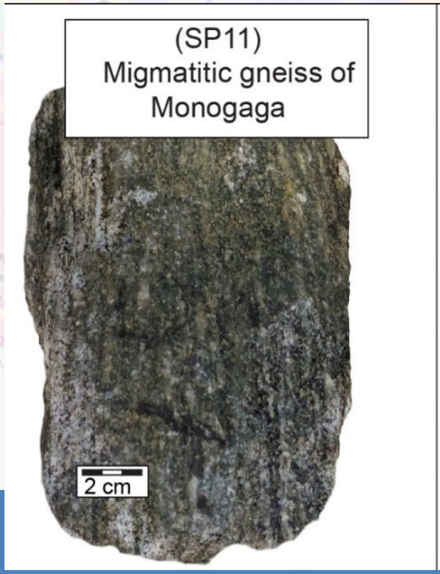

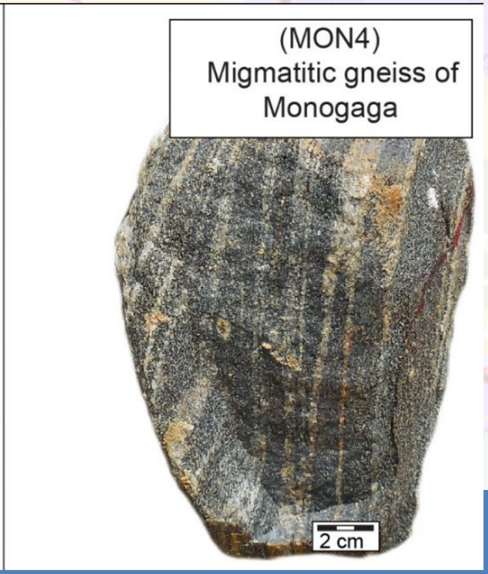

RESULTS

❖ Structural evolution of SASCA domain

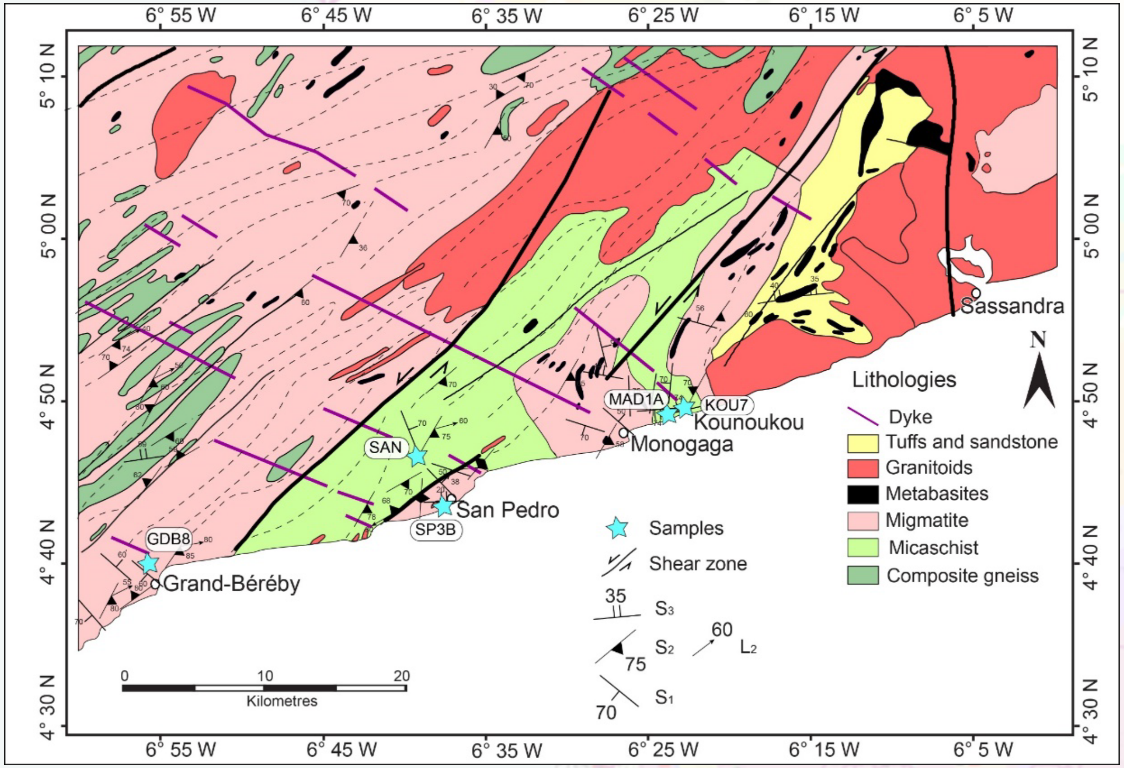

Structural map showing the orientation of S1, S2 and S3 foliations. L2 lineations are also plotted.

D1: NE-SW shortening

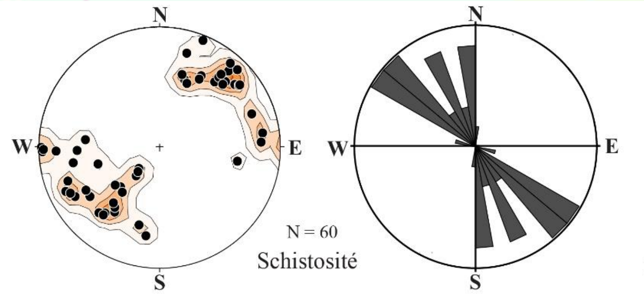

D2: NNW-SSE shortening and Transpressif regime

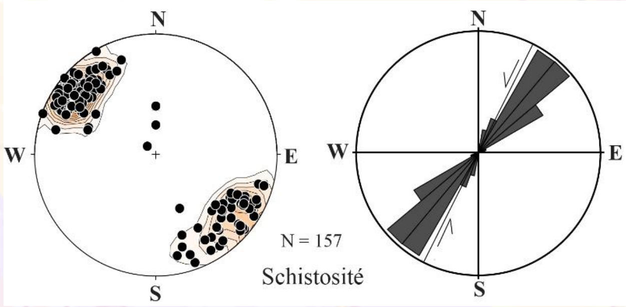

D3: WNW-ESE shortening

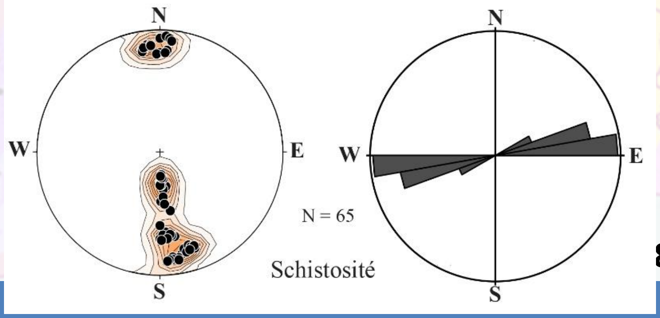

RESULTS

❖ Summary of metamorphic conditions and P-T paths

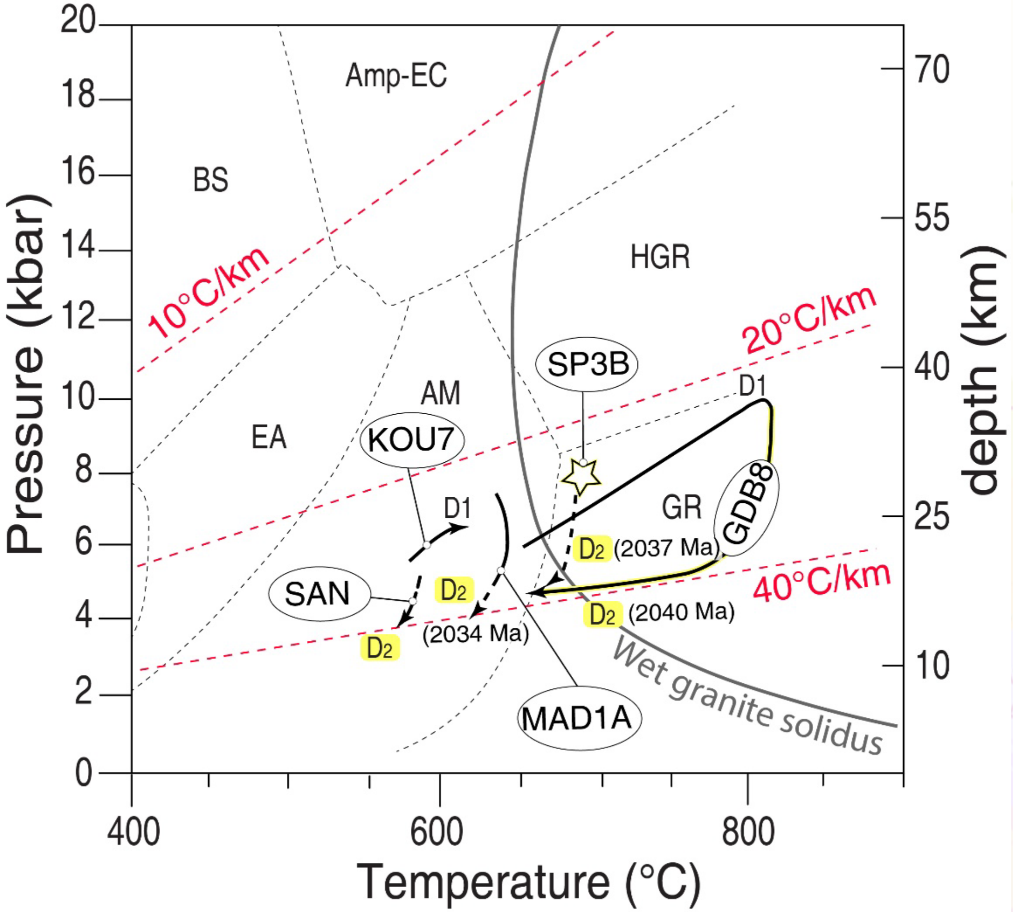

Synthesis of the P–T conditions of the different rocks studied as well as their P–T path according to metamorphic facies and geothermal gradients (modified after Ernst and Liou, 2008). Abbreviations of metamorphic facies: AM: amphibolite; Amp-EC: amphibolite-eclogite; BS: blueschist; EA: epidote amphibolite; GR: sillimanite-granulite; GS: greenschist; HGR: kyanite-granulite.

Garnet–cordierite–sillimanite migmatitic paragneiss (GDB8)

Peak metamorphic: ~ 10 kbar, 820 °C
Decompression from ~ 6 kbar
g-bi-cd-ilm-liq-sill (+q + pl).

Migmatitic grey gneiss (SP3B)

Peak metamorphic: ~ 8-9 kbar, 650-700 °C
g-ilm-q-pl-bi

Staurolite-bearing micaschist (SAN)

~ 570 °C, ~ 4 kbar
st-and-pl-bi-chl-ilm-mt

Garnet–sillimanite–cordierite micaschist (MAD1A)

Decompression to ~ 620-650 °C, 7-8 kbar to 620-690 °C, 5-6 kbar
pl-g-ilm-cd-sill (+q +bi +H_2O)

Garnet–staurolite-bearing micaschist (KOU7)

Peak metamorphic: to ~ 6,6 kbar, 620 °C
pl-g-ilm-st (+q +bi +H_2O)

RESULTS

❖ U–Pb in situ dating of monazite

Garnet–cordierite–sillimanite migmatitic paragneiss (GDB8)

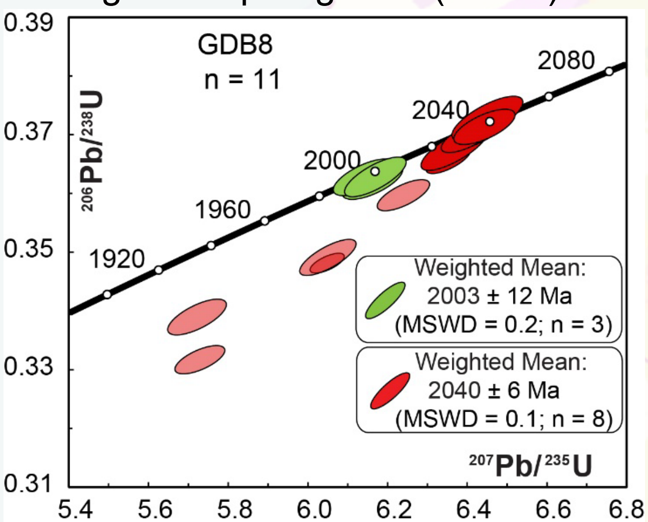

Migmatitic grey gneiss (SP3B)

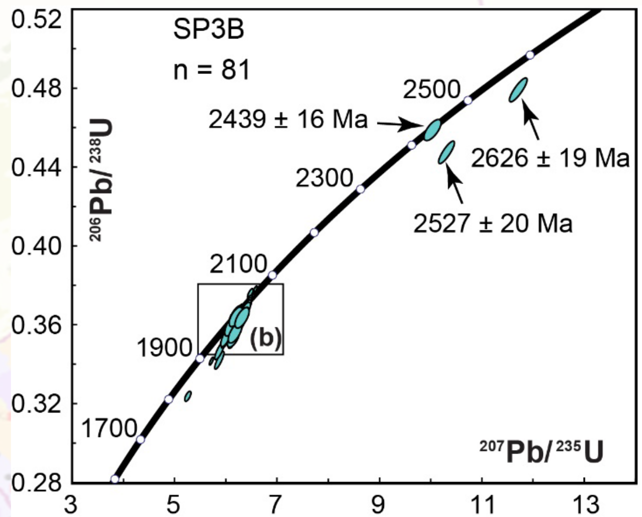

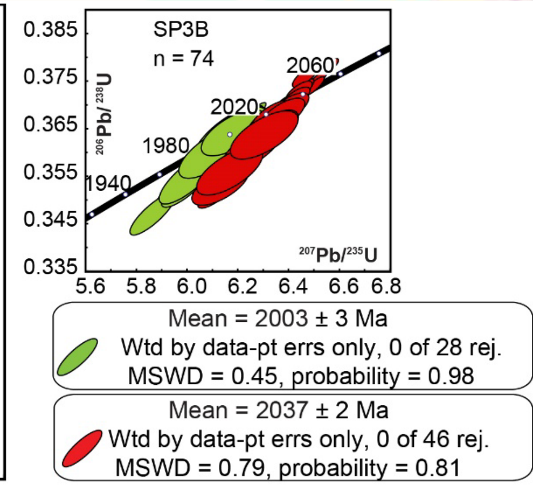

Staurolite-bearing micaschist (SAN)

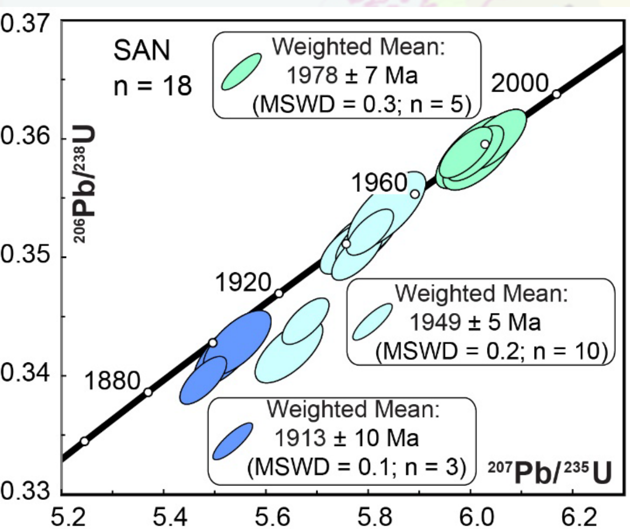

Garnet–sillimanite–cordierite micaschist (MAD1A)

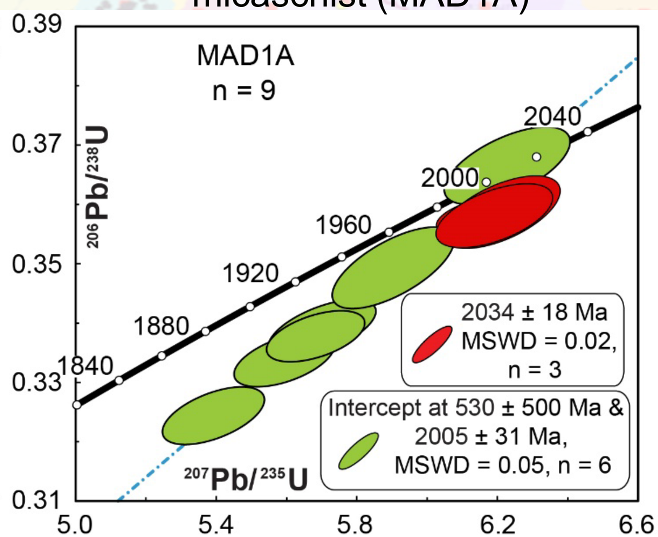

Garnet–staurolite-bearing micaschist (KOU7)

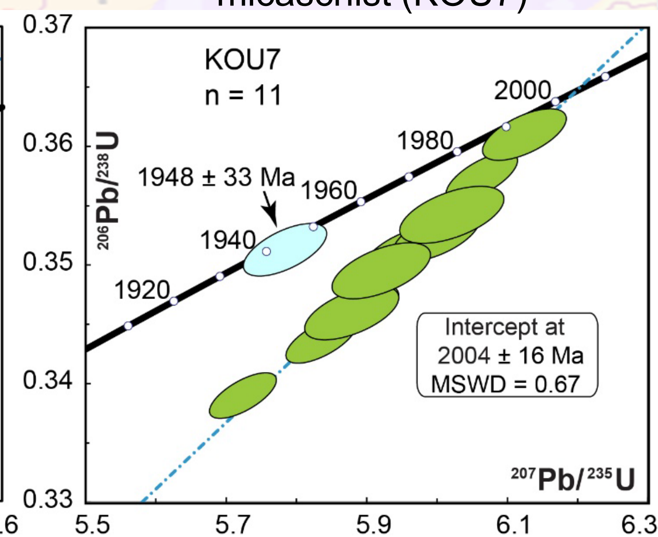

RESULTS

❖ Zircon U-Pb geochronology and Hf isotopes

Archean Gneisses

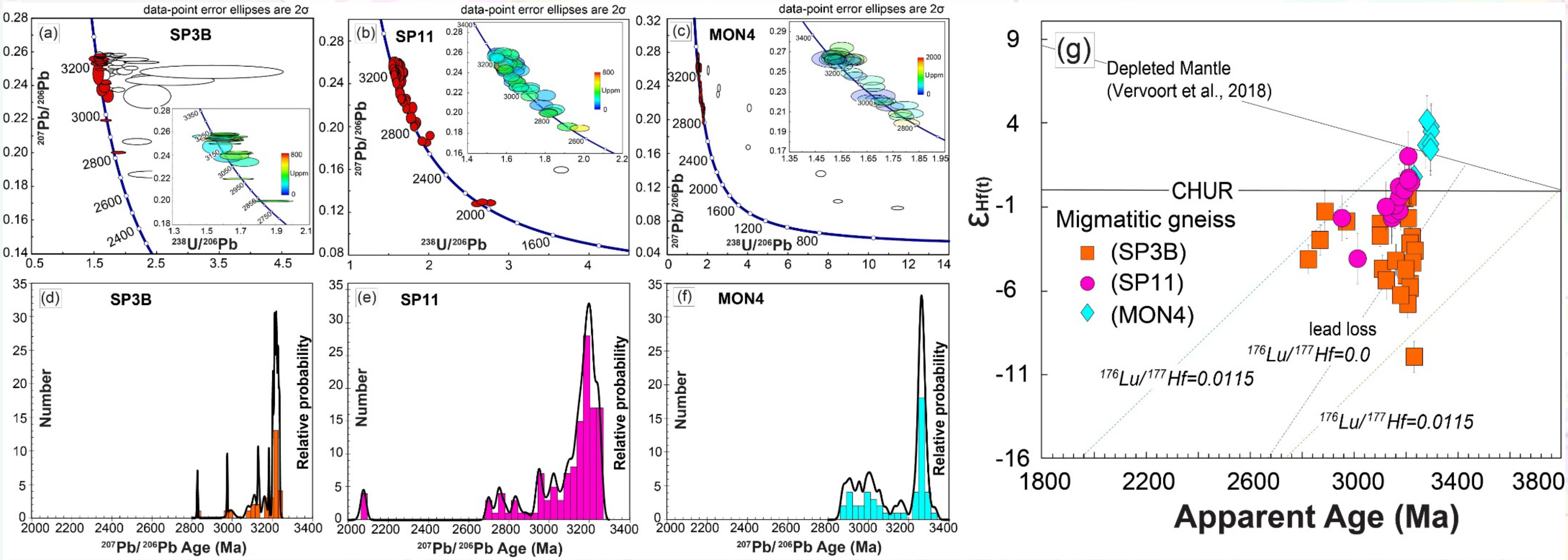

Migmatitic grey gneiss (SP3B)

~3241 Ma to 2827 Ma

subchondritic εHf between - 9.4 and - 0.3 for the age group between 3241 Ma and 3128 Ma.

Migmatitic gneiss (SP11)

1) ~3263 Ma to 2695 Ma

2) ~2082 Ma to 2071 Ma

superchondritic εHf between − 4.1 and + 1.9 zircon cores dated between ca. 3241 and 3078 Ma

Migmatitic gneiss (MON4)

~3328 Ma to 2815 Ma

superchondritic εHf between + 0.7 and + 3.8 comprised between ca. 3230 Ma and 3310 Ma

RESULTS

❖ Zircon U-Pb geochronology and Hf isotopes

Paleoproterozoic Metasediments

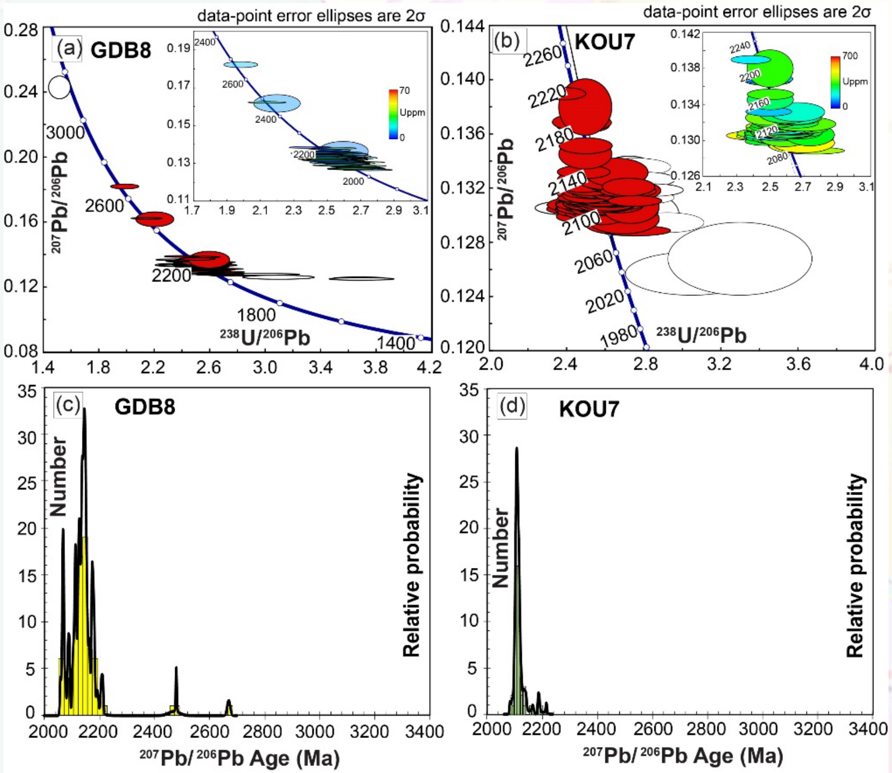

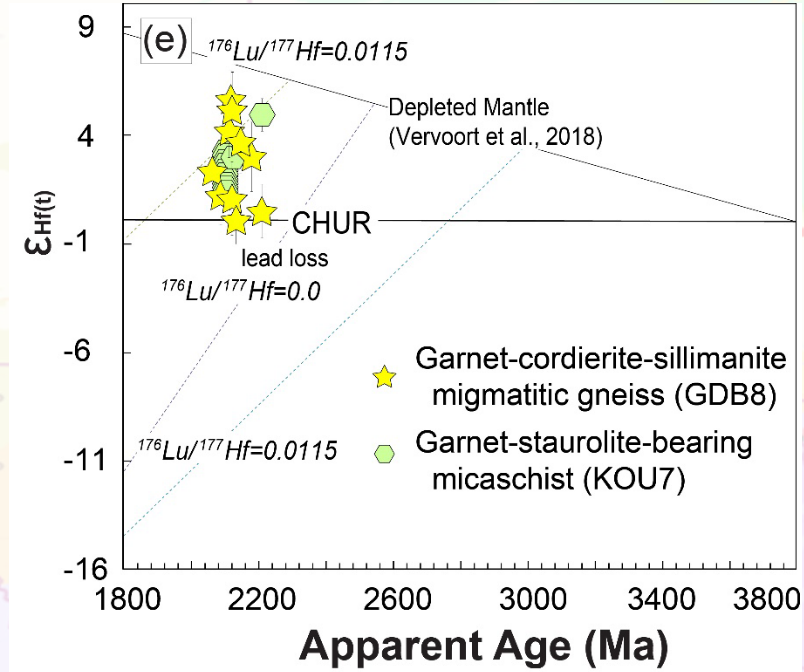

<u>Garnet–cordierite–sillimanite migmatitic paragneiss (GDB8)</u>

1) a single age at 2670 ± 11 Ma
2) two single ages at ca. 2480 Ma and 2472 Ma
3) ~2213 Ma to 2069 Ma

superchondritic εHf between 0.0 and + 5.5 with a detrital sedimentary origin pointing to several sources

<u>Garnet–staurolite-bearing micaschist (KOU7)</u>

~2214 Ma to 2081 Ma

superchondritic εHf between + 1.5 and + 4.9

RESULTS

❖ Zircon U-Pb geochronology and Hf isotopes

Potassic granite (CIS62)

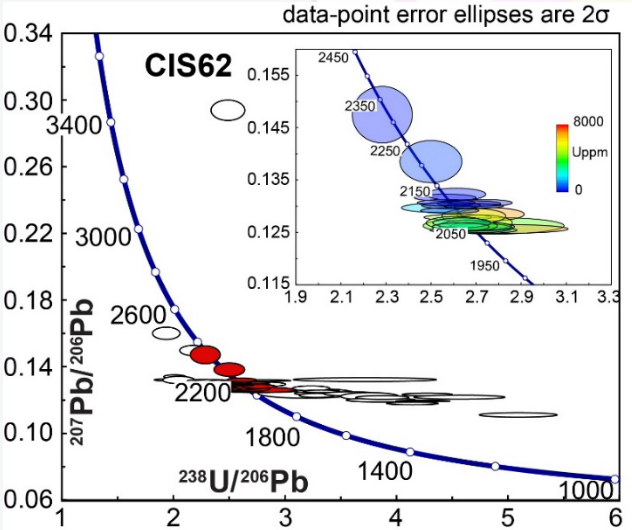

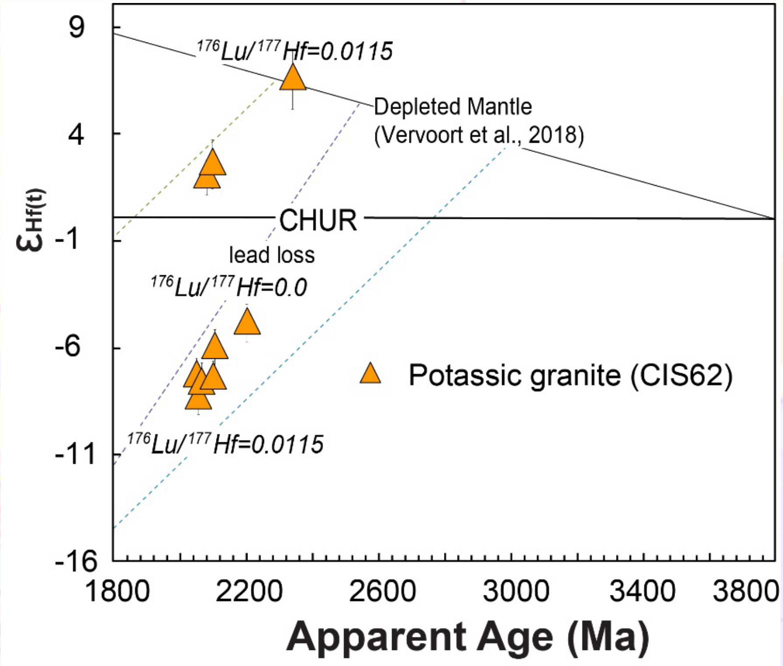

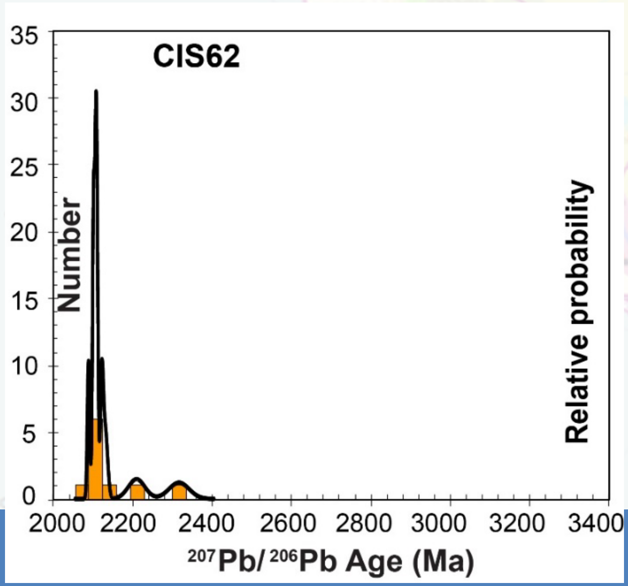

Nine concordant to near concordant analyses spread in ages from ca. 2312 Ma to ca. 2084 Ma.

The date of 2084 ± 6 Ma is tentatively interpreted as the crystalisation age for the potassic granite.

εHf form two distinct clusters between - 4.9 and - 8.5 and between + 1.9 and + 6.5 for zircons formed between ca. 2343 to 2100 Ma.

DISCUSSION

❖ Geodynamic implications for Archean and Paleoproterozoic orogenic processes

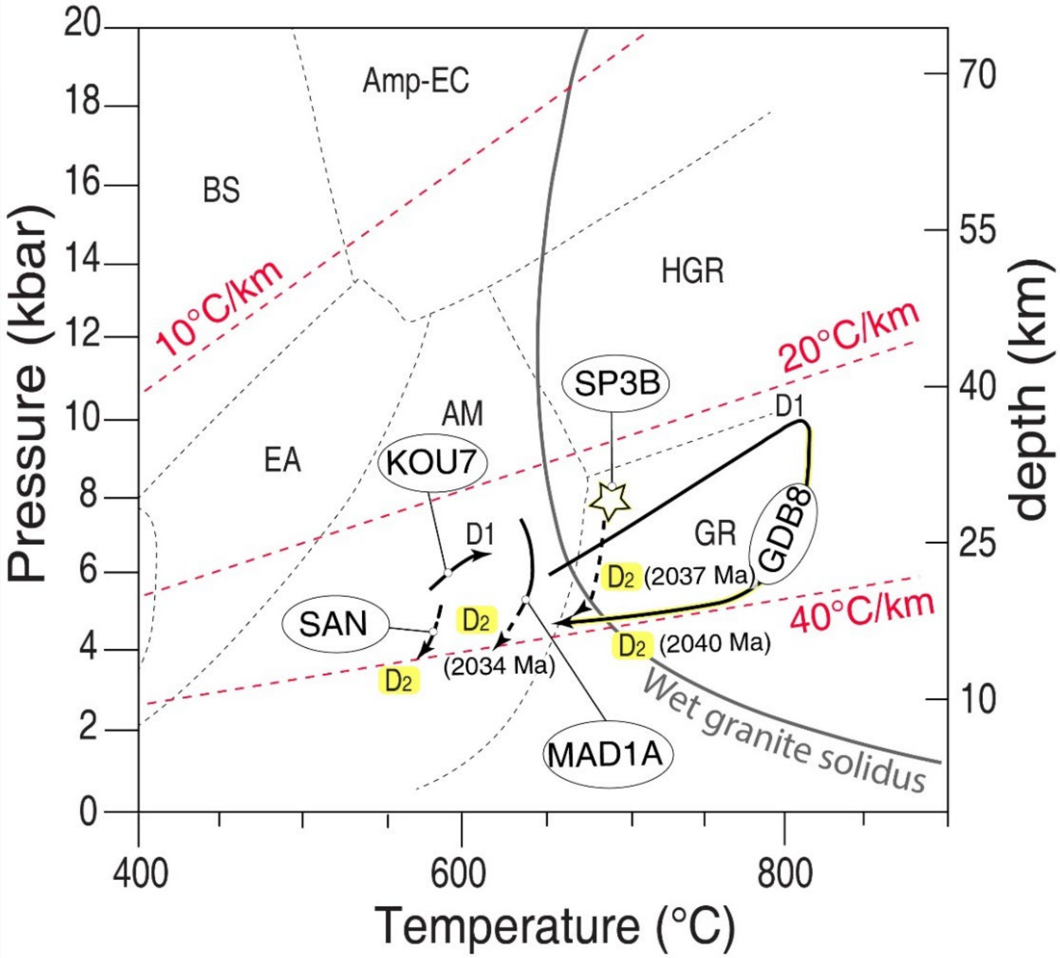

- ✓ thickening of the crust under moderate apparent geothermal gradients of 20–30 °C/km
- ✓ burial of supracrustal rocks in a collision context at the D1 deformation phase before about 2037 Ma
- ✓ metamorphic overprinting from ~ 2070 Ma, documented by younger zircon rims (Koffi et al., 2022)
- ✓ ca. 2037 Ma ages date the retrograde phase D2
- ✓ diversity of metamorphic gradients in the West African Craton (Ganne et al., 2012; Block et al., 2015; McFarlane et al., 2019)

DISCUSSION

❖ Geodynamic implications for Archean and Paleoproterozoic orogenic processes

- ✓ Very young monazites (ca. 2000 Ma and 1978 to 1913 Ma)
- ✓ This is the very first study in the WAC, which determines such young metamorphic ages allowing a correlation with the Guiana Shield where these ages are more abundant.

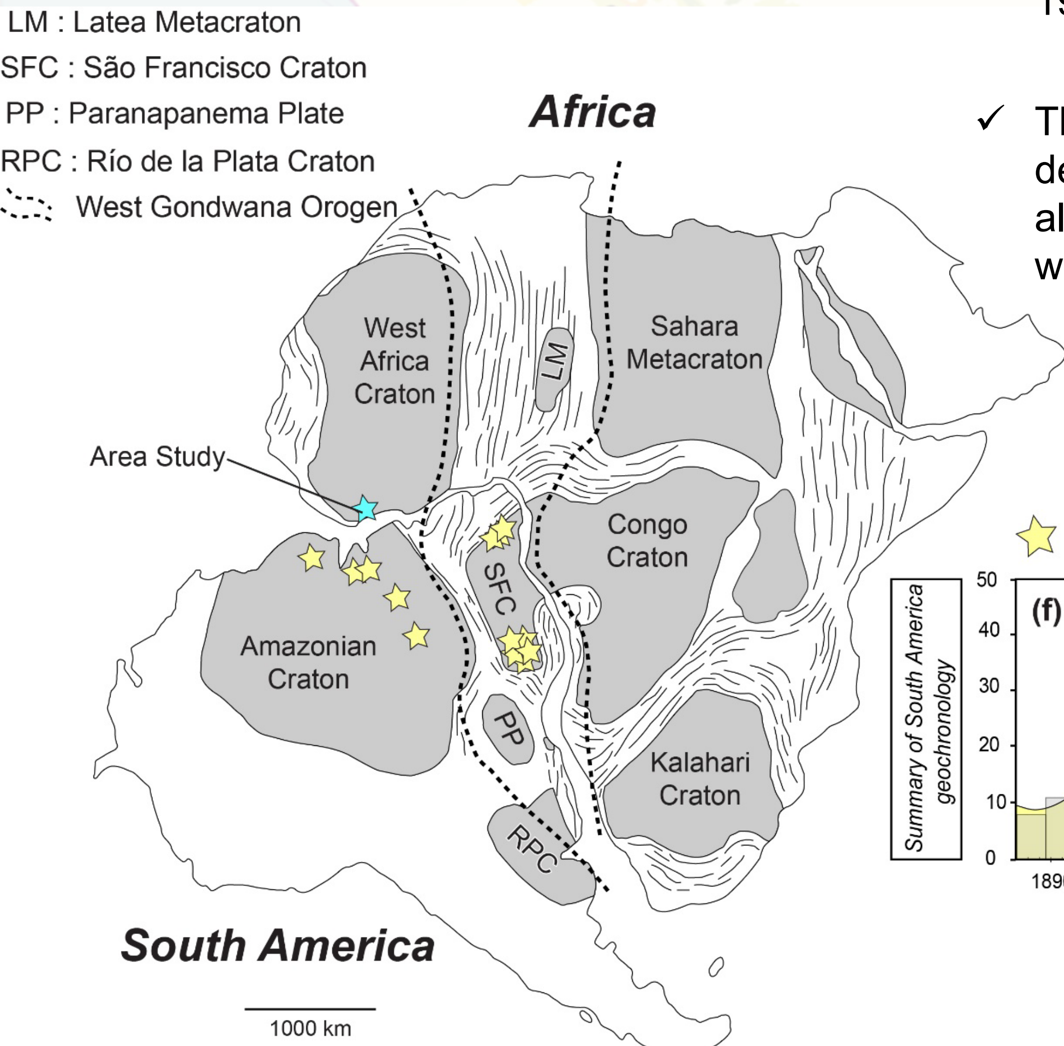

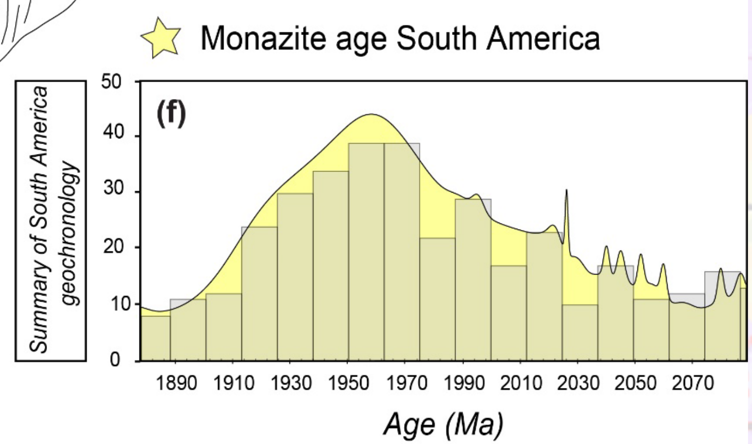

DISCUSSION

❖ Geodynamic implications for Archean and Paleoproterozoic orogenic processes

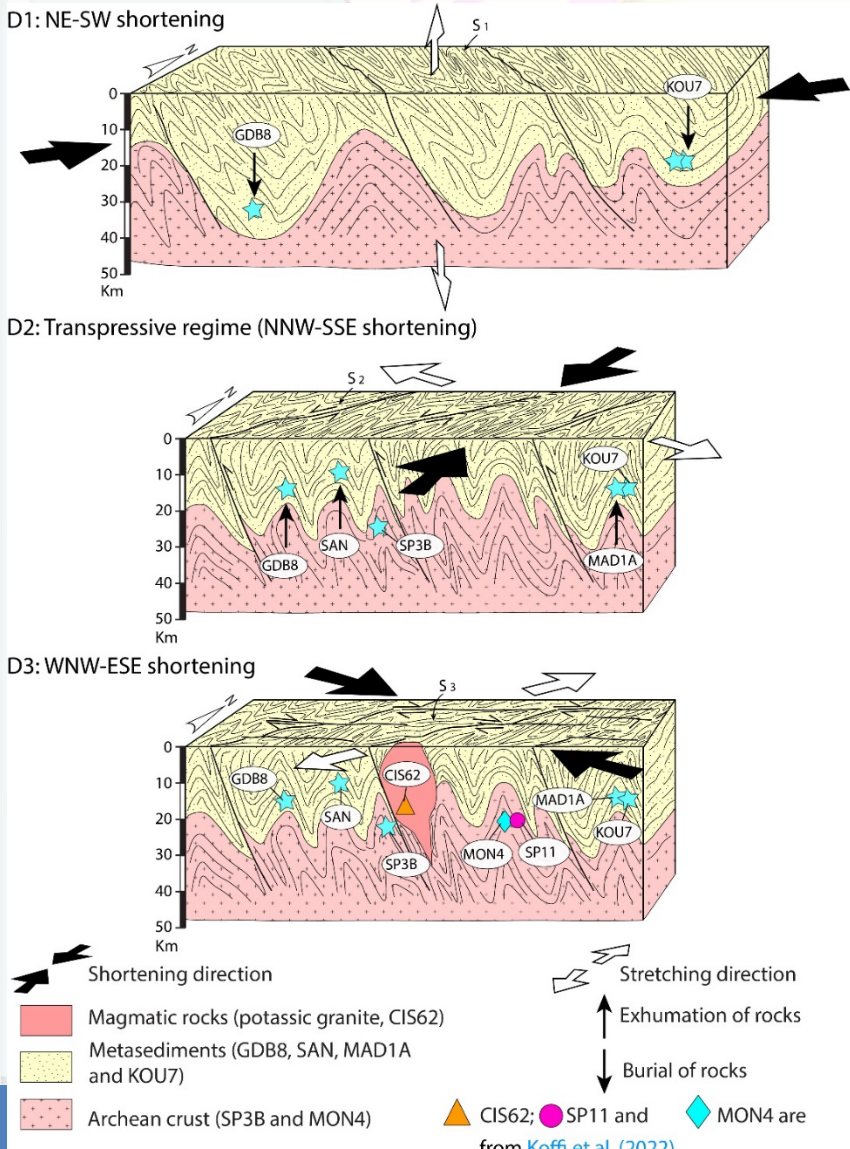

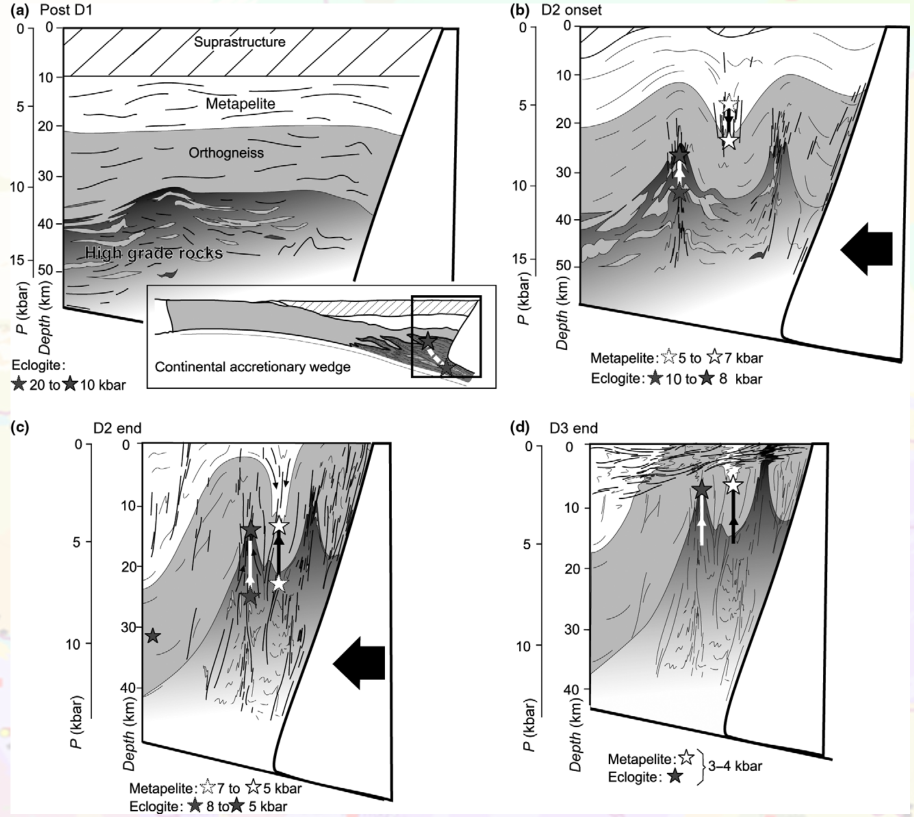

Štípská et al., 2012

DISCUSSION

❖ Geodynamic implications for Archean and Paleoproterozoic orogenic processes

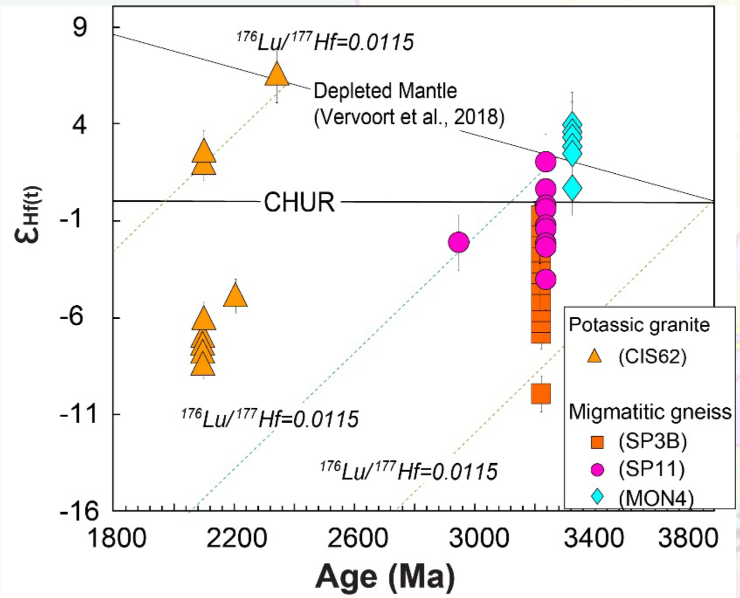

εHf(t) vs $^{207}Pb/^{206}Pb$ age diagrams showing the ages of the protoliths of the San Pedro and Monogaga migmatitic gneisses and the San Pedro potassic granite.

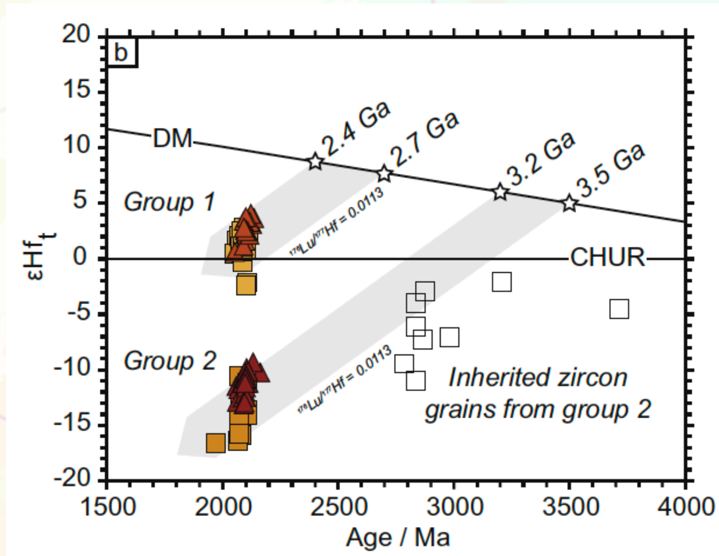

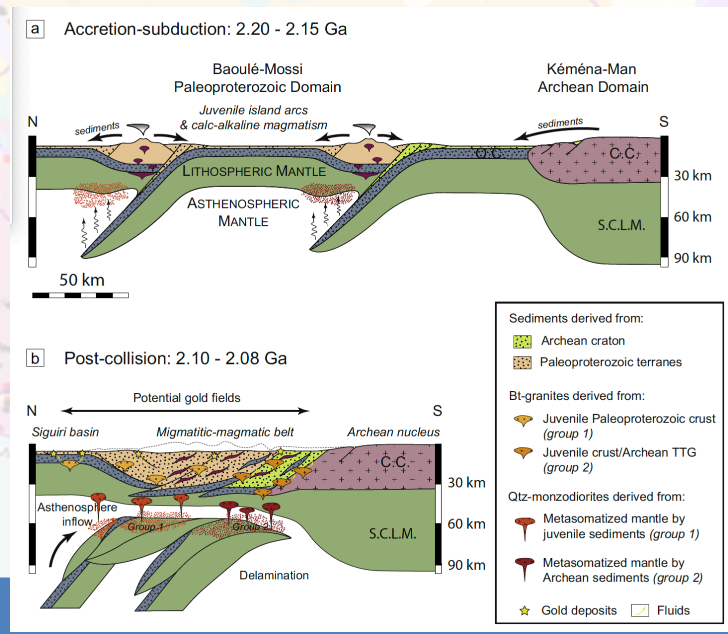

Eglinger et al., 2017

CONCLUSION

- The Sassandra-Cavally (SASCA) domain (SW Côte d'Ivoire) marks the transition between the Archean Kenema-Man craton and the Paleoproterozoic (Rhyacian) Baoule-Mossi domain.

- It is characterized by the tectonic juxtaposition of granulite-facies and amphibolite-facies rocks.

- These conditions are associated with the first recorded deformation D1 and correspond to a Barrovian geothermal gradient of ~25 °C/km. Subsequent exhumation, associated with a second deformation D2, was marked by decompression followed by cooling along apparent geothermal gradients of ~ 40 °C/km at ca. 2037 Ma.

- a model for the tectonic evolution of the SASCA domain at the contact between the Rhyacian Baoule-Mossi domain and the Archean Kenema-Man nucleus whereby crustal thickening is achieved by crustal-scale folding and is followed by and concomitant with lateral flow of the thickened partially molten crust accommodated by regional transcurrent shear zones.

Thank you for your attention